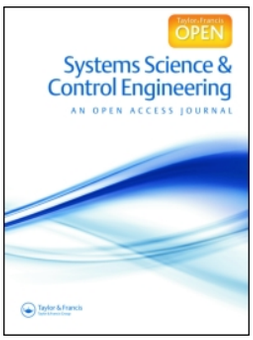

Systems Science & Control Engineering

An Open Access Journal

ISSN: (Print) 2164-2583 (Online) Journal homepage: https://www.tandfonline.com/loi/tssc20

Position feedback dynamic surface control for pneumatic actuator position servo system

Weiyang Lin, Renhe Guan, Letian Yuan, Zhan Li & Mingsi Tong

To cite this article: Weiyang Lin, Renhe Guan, Letian Yuan, Zhan Li & Mingsi Tong (2018) Position feedback dynamic surface control for pneumatic actuator position servo system, Systems Science & Control Engineering, 6:1, 388-397, DOI: 10.1080/21642583.2018.1509400

To link to this article: https://doi.org/10.1080/21642583.2018.1509400

Published online: 22 Aug 2018.

SYSTEMS SCIENCE & CONTROL ENGINEERING: AN OPEN ACCESS JOURNAL
2018, VOL. 6, NO. 1, 388–397
https://doi.org/10.1080/21642583.2018.1509400

Taylor & Francis
Taylor & Francis Group

Position feedback dynamic surface control for pneumatic actuator position servo system

Weiyang Lin[a,b], Renhe Guan[b], Letian Yuan[b], Zhan Li[b] and Mingsi Tong[a,b]

[a]Key Laboratory of Micro-systems and Micro-structures Manufacturing of Ministry of Education, Harbin Institute of Technology, Harbin, China; [b]Research Institute of Intelligent Systems and Control, Harbin Institute of Technology, Harbin, China

ABSTRACT

Pneumatic servo system is widely utilized in many industries, which has huge potential to replace hydraulic and electromechanical system due to its low-cost, high power quality ratio and quick response. There have been considerable control methods proposed to complete pneumatic position servo control. However, these methods still have some inevitable problems which remain to be settled. In this paper, a position feedback dynamic surface control is applied to the pneumatic system based on our pneumatic actuator model in order to provide a new idea for pneumatic position control. Considering model uncertainties, external force disturbance and noise interference, a modified dynamic surface controller is developed to overcome their negative effects. Besides, the stability of the pneumatic system with the modified controller is proved by Lyapunov's stability theorem. Moreover, the results of simulation and pneumatic experiment also verify that the dynamic surface controller is more advantageous than the traditional PID controller in pneumatic position servo control.

ARTICLE HISTORY
Received 19 May 2018
Accepted 5 August 2018

KEYWORDS
Dynamic surface control; pneumatic system; position/force control; position servo

1. Introduction

With high dynamic performance, low pollution, safety and strong environmental adaptability, the servo pneumatic systems are widely used in the industrial automation field. For instance, a pneumatic servo system was designed for packing food products (Wang, Pu, & Moore, 1999). Servo pneumatic actuators were once applied in a climbing robot called Sky Cleaner IV (Zhang, Wang, & Zhang, 2009). Raparelli provided a pneumatic servo mechanism for the rehabilitation of the elbow joint (Raparelli, Ivanov, & Palladino, 2017). Soft pneumatic actuators (SPAs) were utilized as fingers in robotic hands for natural motion and light weight by Tao and Gu (2017). Toyama developed a flat-type pneumatic servo device for mobile robots working in narrow spaces (Toyama & Wakimoto, 2016). An extensor pneumatic muscle actuator for industries was implemented by Al-Ibadi, Nefti-Meziani, and Davis (2017).

However, it is challenging to design a high-performance tracking controller for the pneumatic position servo system, because the precise parameters of the pneumatic system are difficult to be obtained (Ren, Gong, & Li, 2017). Besides, stick-slip of low-speed cylinder, external force disturbance, noise interference and uncertain nonlinear properties of pneumatic system also have adverse effects on the control performance of the system (Schindele & Aschemann, 2009).

To improve accuracy, smoothness and rapidity of the pneumatic system, many engineers and scholars have proposed considerable researches on pneumatic position servo system to find the appropriate and high-performance control method. For example, a Proportion-Integration-Differentiation (PID) controller based on damping optimum was extended by a friction compensation and the stabilization algorithm was designed to achieve precise pneumatic position control in Situm, Pavkovic, and Novakovic (2004). A fuzzy logic controller was implemented for controlling pneumatic servo systems actuated by pneumatic muscle (Sándor, Szabolcs, & József, 2017). A Proportion-Differentiation (PD)-structured fuzzy-pulse width modulation controller was developed using the feedback of the piston position (Fathi & Najafi, 2017). Chiang and Chen accomplished an intelligent adaptive control algorithm by using a neural network to minimize the tracking error (Chiang & Chen, 2017). The paper (Dehghan, Taghizadeh, Surgenor, & Abu-Mallouh, 2011) explored the potential of a novel adaptive on-line neural network compensator for the pneumatic position control.

CONTACT Mingsi Tong tongms@hit.edu.cn

In general, the control of the pneumatic actuator position servo system has always been a complicated issue. There have been a variety of control strategies applied to the pneumatic control including PID control, fuzzy control, neural network control,image-feature-based visual servo control (Tong, Pan, Li, & Lin, 2018) and many other intelligent control methods. However, PID controller lacks rigourous theoretical verification and its parameters cannot be adjusted online. The control accuracy of fuzzy control is low and it requires specialized knowledge and expert experience related to the system. The training speed of neural network control is slow and it is also complex to prove the stability and analyse convergence of such control methods. Therefore, it is quite necessary for us to try new control methods to inspect whether these new methods can solve problems stated above.

In this paper, the dynamic surface control (DSC) of pneumatic system with position feedback is presented. DSC was proposed by Swaroop, Hedrick, Yip, and Gerdes (2000). By using the first-order filter after each step of the backstepping control method, it overcomes the 'explosion of terms' problem caused by the backstepping control method and reduces the amount of calculation remarkably. DSC is effective in controlling uncertain, mismatched nonlinear systems in the strict feedback form. The pneumatic position servo system exactly has many uncertain properties and external disturbance, which can be possibly improved by the DSC method.

The main contribution of this paper is stated as follows. Based on the theories about the pneumatic system, a proper mathematic model on pneumatic position servo system is put forward in this paper. The model can be applied in actual pneumatic control. Then, according to the DSC theory, a dynamic surface controller and a modified dynamic surface controller (MDSC) are designed, which can overcome the negative effects caused by the undesirable characteristics of pneumatic systems. The feasibility of the mathematical model and these designed controllers can be proved by the following actual pneumatic experiments. There is no doubt that the model and controllers will give new reasonable solutions to many pneumatic control problems.

Specifically, this paper is organized as follows. In Section 2, the pneumatic actuator designed by ourselves and the gas flow in the cylinder are modelled. Then, the open loop transfer function between input air pressure and output displacement of cylinder rod is set up. In Section 3, a dynamic surface controller is designed for the pneumatic actuator based on the models established in the previous section. Next, to eliminate modelling uncertainties and resist force and noise interference, a robust and adaptive DSC is proposed. What is more, by constructing Lyapunov functions, stability conditions of these two methods are obtained, respectively. In Section 4, the feasibility of our control method is verified by the experiment. From the results of the experiment, it is obvious that compared to the traditional PID algorithm, the DSC method has better control performance and stronger robustness.

2. The mathematical model of pneumatic actuator

In order to control the pneumatic actuator, it is essential to establish its mathematical model. The model can be described as the following equations: force equilibrium equation of the pneumatic actuator, mass flow equation of cylinder chamber and pressure equation of cylinder chamber. According to these equations, the open loop transfer function of the pneumatic actuator is built. By controlling the input pressure of the cylinder and eliminating bad effects of contact force interference, the cylinder can output expected displacement.

2.1. Force equilibrium equation of pneumatic actuator

The schematic diagram of the pneumatic system is shown in Figure 1. Consider the mass of moving platform as M_p, the total mass of the end pneumatic actuator as m, the output force of the pneumatic actuator as F_1, the force between M and m as F_2, the contact force from workpiece as F_L and the angle between the actuator and vertical direction as α. The photograph of the actuator is shown in Figure 2. As the photograph illustrates, the actuator is driven by the cylinder and it realizes reciprocating motion by changing the pressure of two chambers.

On the basis of Newton's second law, force equilibrium equation of pneumatic actuator can be obtained:

$$F_1 + F_2 - F_L + G_\alpha - f - K_v\dot{x} = m\ddot{x} \tag{1}$$

where G_α is the component of the gravity of m in the α direction, which can be calculated by $G_\alpha = mg\sin\alpha$, f is the Coulomb friction, x is the displacement of the cylinder rod and K_v is the viscous friction coefficient.

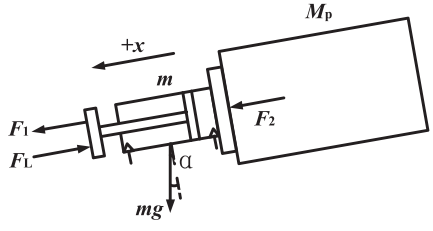

Figure 1. Force analysis of the pneumatic system.

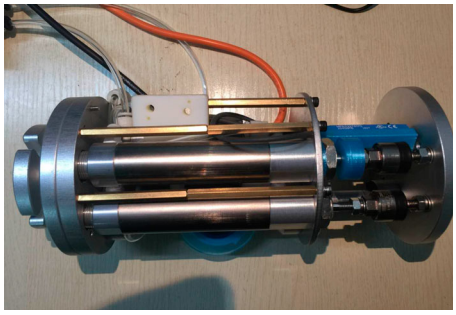

Figure 2. Photograph of the pneumatic actuator.

2.2. Mass flow equation of cylinder chambers

Assume that the gas flow is continuous, it can be deduced that the changing rate of gas mass flow is equal to the difference between the mass flow rate flowing in and out. Let $M = \rho \cdot V$ denote the mass flow and the following equation is obtained:

$$\dot{M}_{\text{in}} - \dot{M}_{\text{out}} = \rho \frac{\mathrm{d}V}{\mathrm{d}t} + V \frac{\mathrm{d}\rho}{\mathrm{d}t} \tag{2}$$

Then, take the ideal gas equation $\rho = (p/RT)$ into Equation (2):

$$\begin{aligned} \dot{M}_{\text{in}} &= \frac{1}{RT_1}\left(p_1 \frac{\mathrm{d}V_1}{\mathrm{d}t} + V_1 \frac{\mathrm{d}p_1}{\mathrm{d}t} - \frac{p_1 V_1}{T_1}\frac{\mathrm{d}T_1}{\mathrm{d}t}\right) \\ \dot{M}_{\text{out}} &= \frac{1}{RT_2}\left(p_2 \frac{\mathrm{d}V_2}{\mathrm{d}t} + V_2 \frac{\mathrm{d}p_2}{\mathrm{d}t} - \frac{p_2 V_2}{T_2}\frac{\mathrm{d}T_2}{\mathrm{d}t}\right) \end{aligned} \tag{3}$$

where signs with subscript 1 are all related to intake chamber of the cylinder, while subscript 2 represents the exhaust chamber. Besides, subscript 0 represents the initial condition and S stands for the effective area of chambers.

Suppose that the whole process is adiabatic and k is the specific heat ratio, the relationship between the varying temperature T and its initial value T_0 can be described as:

$$T_i = T_{i0}\left(\frac{p_i}{p_{i0}}\right)^{(k-1/k)} \tag{4}$$

where $i = 1, 2$. Then, take the derivation of Equation (4) with respect to time and plug it into Equation (3). Therefore, for intake chamber and exhaust chamber of the cylinder, there exist two equations, respectively:

$$\begin{aligned} \dot{M}_{\text{in}} &= \frac{1}{RT_1}\left(p_1 \frac{\mathrm{d}V_1}{\mathrm{d}t} + \frac{V_1}{k}\frac{\mathrm{d}p_1}{\mathrm{d}t}\right) \\ \dot{M}_{\text{out}} &= \frac{1}{RT_2}\left(p_2 \frac{\mathrm{d}V_2}{\mathrm{d}t} + \frac{V_2}{k}\frac{\mathrm{d}p_2}{\mathrm{d}t}\right) \end{aligned} \tag{5}$$

Assume that $S_1 P_{10} = S_2 P_{20}$, $T_{10} = T_{20} = T_0$ and the piston only moves around the middle. Set the effective area ratio of the two chambers as $n = S_2/S_1$ and the initial volume ratio of the two chambers as $r = V_{20}/V_{10}$, the mass flow rate in the intake chamber and the exhaust chamber can be expressed as:

$$\begin{aligned} \dot{M}_{\text{in}} &= \frac{1}{RT_0 k}\left(kS_1 p_1 \frac{\mathrm{d}V_1}{\mathrm{d}t} + V_{10}\frac{\mathrm{d}p_1}{\mathrm{d}t}\right) \\ \dot{M}_{\text{out}} &= \frac{1}{RT_0 k}\left(kS_2 p_2 \frac{\mathrm{d}V_2}{\mathrm{d}t} + rV_{10}\frac{\mathrm{d}p_2}{\mathrm{d}t}\right) \end{aligned} \tag{6}$$

2.3. Equations of the pressures of two cylinder chambers

Suppose that L is the length of stroke. The pressure differential equation of the cylinder can be obtained. According to the first law of thermodynamics, the energy equation of two cylinder chambers can be simplified as follows:

$$\begin{aligned} \frac{\mathrm{d}p_1}{\mathrm{d}t} &= RkT_0 \frac{\dot{M}_1}{V_1} - \frac{kp_1 \dot{x}}{x} \\ \frac{\mathrm{d}p_2}{\mathrm{d}t} &= RkT_0 \frac{\dot{M}_2}{V_2} - \frac{kp_2 \dot{x}}{L - x} \end{aligned} \tag{7}$$

2.4. Transfer function of compliant system

The mass flow through the valve is the function of the size of the opening area X_{v}, intake pressure p_{u}, exhaust pressure p_{d}, intake temperature T_{u} and exhaust temperature T_{d}. Accordingly, the function can be written as:

$$\dot{M}_i = p_{\text{u}} X_{\text{v}} \rho \sqrt{\frac{T_{\text{u}}}{T_{\text{d}}}} \psi_i(p_{\text{u}}, p_{\text{d}}) \tag{8}$$

where

$$\psi_i(p_{\text{u}}, p_{\text{d}}) = \begin{cases} 1 & , \frac{p_{\text{d}}}{p_{\text{u}}} > b \\ \sqrt{1 - \left(\frac{\frac{p_{\text{d}}}{p_{\text{u}}} - b}{1 - b}\right)^2} & , \frac{p_{\text{d}}}{p_{\text{u}}} \le b \end{cases} \tag{9}$$

and b is a constant which stands for the critical pressure ratio.

In our system, the mass flow is mainly affected by the intake pressure p_{c} which is also the input of our system and exit pressure p_i of the valve, because the valve selected is an electromagnetic valve and the opening area is constant while opening. Linearize with the Tylor formula (Lin, Dong, Deng, Qian, & Qiu, 2016),

$$\begin{aligned} \dot{M}_1 &= K_{p_{\text{a}}} p_{\text{c}} - K_{C_{\text{a}}} p_1 \\ \dot{M}_2 &= K_{p_{\text{b}}} p_{\text{c}} - K_{C_{\text{b}}} p_2 \end{aligned} \tag{10}$$

where

$$K_{p_a} = \frac{\partial \dot{M}_1}{\partial p_c}\bigg|_{p_c=0}, \quad K_{p_b} = \frac{\partial \dot{M}_2}{\partial p_c}\bigg|_{p_c=0},$$
$$K_{C_a} = \frac{\partial \dot{M}_1}{\partial p_1}\bigg|_{p_1=0} \text{ and } K_{C_b} = \frac{\partial \dot{M}_2}{\partial p_2}\bigg|_{p_2=0}.$$

Actually, the dynamic response of the valve is much faster than that of mechanical systems. Therefore, we concentrate more on the dynamic characteristics of pneumatic system as well as on the load of the cylinder and ignore the dynamic characteristics of the valve. Assuming the pressure of the load is $p_L = p_1 - np_2$, the output force F_1 can be expressed as $F_1 = p_L S_1$ and the force equilibrium equation analysed previously can be written in the following form:

$$\left(K_{p_a} + \frac{n}{r}K_{p_b}\right)p_c - \left(\frac{n}{r}K_{C_b} + nK_{Ca}\right)p_2 + K_{C_a}p_L = \frac{1}{RT_0k}\left[\left(\frac{dp_1}{dt} - n\frac{dp_2}{dt}\right)V_{10} + (1 + dfracnr)\,kS_1p_{10}\frac{dx}{dt}\right] \tag{11}$$

then, take Laplace transformation of Equations (1) and (11),

$$\left(K_{p_a} + \frac{n}{r}K_{p_b}\right)p_c(s) - \left(\frac{n}{r}K_{C_b} + nK_{C_a}\right)p_2(s) - \frac{1}{RT}\left(1 + \frac{n}{r}\right)S_1p_{10}sx(s) = \left(K_{C_a} + \frac{sV_{10}}{RT_0k}\right)p_L(s) \tag{12}$$

$$F_1(s) = (ms^2 + K_v s)x(s) + f(s) + F_L(s) - G_\alpha(s) - F_2(s) \tag{13}$$

Since when the valve is open, p_b is nearly constant about one standard atmospheric pressure. Therefore, $p_2(s)$ can be regarded as zero. Let

$$\beta_n = S_1^2P_{10}kr + S_1^2P_{10}kn + K_{c_a}K_vRT_0kr \tag{14}$$

then, the transfer function $A(s)$ between $x(s)$ and $p_c(s)$ can be obtained:

$$\frac{x(s)}{p_c(s)} = \frac{S_1RT_0k(K_{c_b} + K_{c_a}r)}{mV_{10}rs^3 + (K_{c_a}RT_0kmr + K_vV_{10}r)s^2 + \beta_n s} \tag{15}$$

let $F_w = F_L + f - G_\alpha - F_2$ and the transfer function $B(s)$ between $x(s)$ and $F_w(s)$ can be acquired:

$$\frac{x(s)}{F_w(s)} = \frac{RT_0kr}{mV_{10}rs^3 + (K_{c_a}RT_0kmr + K_vV_{10}r)s^2 + \beta_n s} \tag{16}$$

In addition,

$$x(s) = A(s)p_c(s) + B(s)F_w(s) \tag{17}$$

for ease of analysis, Equation (15) can be simplified as:

$$\frac{x(s)}{p_L(s)} = \frac{K_1}{As^3 + Bs^2 + Cs} \tag{18}$$

similarly,

$$\frac{x(s)}{F_w(s)} = \frac{K_2}{As^3 + Bs^2 + Cs} \tag{19}$$

In the process of establishing the mathematical model, it may be difficult to get the linear parameters K_{p_a} and K_{p_b}. However, as seen in Equations (15) and (16), these two parameters are finally not relevant to the final transfer functions. Taking other necessary parameters stated in the former part into transfer function equations, the specific transfer function can finally be obtained. Normally, the parameter C in Equations (18) and (19) is much larger than the parameter B and A, while the parameters K_1 and K_2 are close to C.

3. Control algorithm of the pneumatic actuator

3.1. Dynamic surface control

Let $F_w = 0$, the analysis can be simplified. Transfer Equation (17) into the state-space form,

$$\begin{aligned} \dot{x}_1 &= x_2 \\ \dot{x}_2 &= x_3 \\ \dot{x}_3 &= \frac{1}{A}(K_1P_L(t) - Cx_2 - Bx_3) \\ x &= x_1 \end{aligned} \tag{20}$$

The main purpose of the DSC is to design a state feedback control law u in order that output x tracks the desired trajectoryx_1^d.

To avoid 'explosion of terms' problem caused by backstepping control, the DSC algorithm allows one virtual control variable in backstepping control to pass through a first-order filter and constructs another control variable. Based on this method, the DSC controller is designed in the following.

First step: design the surface function $S_1 = x_1 - x_1^d$, then its dynamic function can be written as:

$$\dot{S}_1 = x_2 - \dot{x}_1^d \tag{21}$$

define virtual control variable α_2 as

$$\alpha_2 = -k_1S_1 + \dot{x}_1^d \tag{22}$$

where k_1 is an adjustable parameter for stabilizing the controller. In order to eliminate derivative terms produced by the derivation of virtual control variables, let α_2

pass through a first-order filter and then a new parameter variable x_2^d is produced, where τ_2 is the filter time constant.

$$\tau_2 \dot{x}_2^d + x_2^d = \alpha_2 \tag{23}$$

Second step: similarly, the surface function $S_2 = x_2 - x_2^d$ can be obtained and the dynamic function is as follows:

$$\dot{S}_2 = x_3 - \dot{x}_2^d \tag{24}$$

besides, virtual control variable α_3 is

$$\alpha_3 = -k_2 S_2 + \dot{x}_2^d \tag{25}$$

k_2 is also an adjustable parameter for stabilizing the controller. Then, let α_3 pass through a first-order filter and τ_3 is the filter time constant.

$$\tau_3 \dot{x}_3^d + x_3^d = \alpha_3 \tag{26}$$

Third step: the last surface function is $S_3 = x_3 - x_3^d$, and the control law is

$$u = \frac{1}{\lambda}\left(-k_3 S_3 + \frac{C}{A}x_2 + \frac{B}{A}x_3 + \dot{x}_3^d\right) \tag{27}$$

so far, the dynamic surface controller has already been designed.

3.2. Lyapunov stability verification of DSC controller

Define filtering variable $z_2 = x_2^d - \alpha_2 = -\tau_2 \dot{x}_2^d$ and similarly filtering variable $z_3 = x_3^d - \alpha_3 = -\tau_3 \dot{x}_3^d$. Then, the Lyapunov function of the dynamic surface controller is constructed,

$$V(S_i, z_i) = \frac{1}{2}(S_1^2 + S_2^2 + S_3^2) + \frac{1}{2}(z_2^2 + z_3^2) \tag{28}$$

When the function V is equal to zero, the actual and expected motion state of the object is static. However, the object cannot be static all the time in actual circumstances. Therefore, the function V is larger than zero. Next, take the derivation of Equation (28),

$$\dot{V}(S_i, z_i) = S_1\dot{S}_1 + S_2\dot{S}_2 + S_3\dot{S}_3 + z_2\dot{z}_2 + z_3\dot{z}_3 \tag{29}$$

In order to obtain the negative derivative of the Lyapunov function, it is necessary to simplify $S_i\dot{S}_i$ and $z_i\dot{z}_i$. When $i = 1,2$, $S_i\dot{S}_i$ can be simplified as:

$$\begin{aligned} S_i\dot{S}_i &= S_i(\dot{x}_i - \dot{x}_i^d) \\ &= S_i(x_{i+1} - \alpha_{i+1} - k_i S_i) \\ &= S_i(z_{i+1} - x_{i+1}^d + x_{i+1} - k_i S_i) \\ &= S_i(z_{i+1} + S_{i+1} - k_i S_i) \\ &= S_i z_{i+1} + S_i S_{i+1} - k_i S_i^2 \end{aligned} \tag{30}$$

particularly, when $i = 3$, $S_3\dot{S}_3 = -k_3 S_3^2$, $z_4 = 0$, $\alpha_4 = 0$, $x_4^d = 0$ and $x_4 = 0$, since the system is the third order. For convenience, write $\dot{x}_i$ as $\dot{x}_i = x_{i+1} + f_i(x_1, x_2, x_3)$, where $i = 1,2$. When $i = 3$, $\dot{x}_3 = \lambda u + f_3(x_1, x_2, x_3)$, where $\lambda = (K_1/A)$. Then simplify $z_i\dot{z}_i$. According to the property of the filter, the following equation can be attained:

$$\tau_{i+1}\dot{x}_{i+1}^d + x_{i+1}^d = -k_i S_i - f_i(x_1, x_2, x_3) + \dot{x}_i^d \tag{31}$$

take the derivation of Equation (31),

$$\tau_{i+1}\ddot{x}_{i+1}^d + \dot{x}_{i+1}^d = -k_i\dot{S}_i - \Sigma\frac{\partial f_i}{\partial x_k}\dot{x}_k + \ddot{x}_i^d \tag{32}$$

Combine Equations (31) and (32), then we can get

$$\begin{aligned} \dot{z}_{i+1} &= -\frac{z_{i+1}}{\tau_{i+1}} + k_i\dot{S}_i + \Sigma\frac{\partial f_i}{\partial x_k}\dot{x}_k - \ddot{x}_i^d \\ &= -\frac{z_{i+1}}{\tau_{i+1}} + \phi_{i+1}(S_i, x_i) \end{aligned} \tag{33}$$

where $\phi_{i+1}(S_i, x_i) = k_i\dot{S}_i + \Sigma((\partial f_i)/(\partial x_k))\dot{x}_k - \ddot{x}_i^d$. Besides, $z_i\dot{z}_i$ can be represented as

$$z_{i+1}\cdot\dot{z}_{i+1} = -\frac{z_{i+1}^2}{\tau_{i+1}} + z_{i+1}\cdot\phi_{i+1}(S_i, x_i) \tag{34}$$

then Equation (29) can be transformed as

$$\begin{aligned} \dot{V}(S_i, z_i) = &- k_1 S_1^2 - k_2 S_2^2 - k_3 S_3^2 - \frac{z_2^2}{\tau_2} - \frac{z_3^2}{\tau_3} \\ &+ S_1 z_2 + S_1 S_2 + S_2 z_3 + S_2 S_3 + z_2\phi_2 + z_3\phi_3 \end{aligned} \tag{35}$$

Assume that $V(0)$ is the initial state of the Lyapunov function and p is an upper bound of it. It is obvious that x_i^d and its all-order derivative are bounded, because x_i^d is the desired trajectory set by ourselves. Then, consider the following two compact sets Ω_1 and Ω_2:

$$\begin{aligned} \Omega_1 &= \{(x_i^d, \dot{x}_i^d, \ddot{x}_i^d) : (x_i^d)^2 + (\dot{x}_i^d)^2 + (\ddot{x}_i^d)^2 < \zeta\} \\ \Omega_2 &= \{(S_i, z_i) : S_1^2 + S_2^2 + S_3^2 + z_2^2 + z_3^2 < 2p\} \end{aligned} \tag{36}$$

If the function ϕ_i belongs to the compact set $\{\Omega_1 \times \Omega_2\}$, it has the upper bound which can be set as M_i. According to Young's inequality,

$$\begin{aligned} &S_1 z_2 + S_1 S_2 + S_2 z_3 + S_2 S_3 + z_2\phi_2 + z_3\phi_3 \le S_1^2 + \\ &\frac{3}{2}S_2^2 + \frac{1}{2}S_3^2 + \frac{1}{2}z_2^2 + \frac{1}{2}z_3^2 + \frac{1}{2}z_2^2\phi_2^2 + \frac{1}{2}z_3^2\phi_3^2 + 1 \end{aligned} \tag{37}$$

therefore,

$$\begin{aligned} \dot{V}(S_i, z_i) \le\ & S_1^2(-k_1 + 1) + S_2^2\left(-k_2 + \frac{3}{2}\right) \\ &+ S_3^2\left(-k_3 + \frac{1}{2}\right) + z_2^2\left(-\frac{1}{\tau_2} + \frac{1}{2} + \frac{1}{2}\phi_2^2\right) \\ &+ z_3^2\left(-\frac{1}{\tau_3} + \frac{1}{2} + \frac{1}{2}\phi_3^2\right) \end{aligned} \tag{38}$$

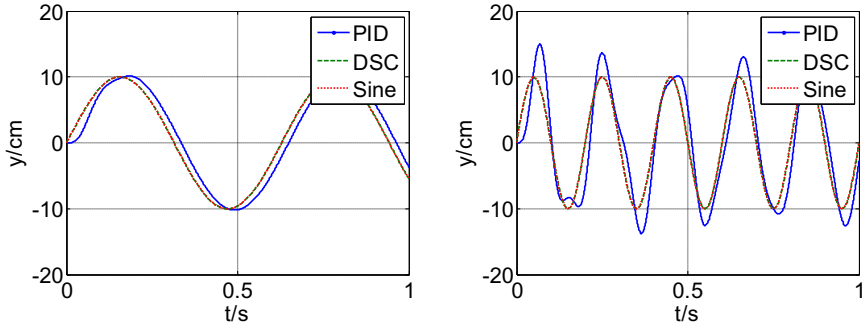

Figure 3. Simulation results of sine signal.

select $b > 0, k_1 \geq 1 + b, k_2 \geq \frac{3}{2} + b, k_3 \geq \frac{1}{2} + b, (1/\tau_2) \geq (M_2^2/2) + \frac{1}{2} + b, (1/\tau_3) \geq (M_3^2/2) + \frac{1}{2} + b$, then

$$\dot{V} \leq -2bV + 1 + \left(\frac{M_2^2\phi_2^2}{2M_2^2} - \frac{M_2^2}{2}\right) z_2^2 + \left(\frac{M_3^2\phi_3^2}{2M_3^2} - \frac{M_3^2}{2}\right) z_3^2 \tag{39}$$

Since $V(0) \leq p$ and M_i is the upper bound of ϕ_i, the latter two items are not greater than zero. Set $b > (1/2p)$, then, $\dot{V} < 0$ can be easily verified. Therefore, the function V is smaller than p and it also belongs to the compact sets. Thus, if the related parameters in the former equations satisfy the certain conditions, the control method can be stable.

3.3. Simulation research of DSC

To test the effect of the DSC controller, a simulation experiment is designed to compare the performance between the traditional PID controller and DSC controller when a reference sine signal, a step signal and a ramp signal are input into the system. In the simulation, the amplitude of sine input is set as 10 cm and the frequency as 1.6 Hz and 5 Hz. The method of simulation is thefourth-order Runge–Kutta method and the total simulation time is 1 s with the sampling time of 0.001 s. The simulation results of sine signal are shown in Figure 3. The left one is about 1.6 Hz sine signal and the right one is about 5 Hz sine signal. Besides, the results of step input and ramp input are shown in Figure 4.

From the results, the traditional PID controller can track the sine signal approximately when the frequency of the input sine is 1.6 Hz while it cannot track the sine signal with 5 Hz frequency. However, the DSC controller can accomplish the task of tracking the input sine signals with 1.6 Hz and 5 Hz, which proves that it has a greater bandwidth than the traditional PID controller. When it comes to step signal and ramp signal, the DSC controller has a faster response speed, smaller steady-state error and less overshoot.

3.4. Lyapunov stability verification of MDSC controller

The proving process is similar to the previous one. Similarly, consider filtering variable as $z_i = x_i^{\mathrm{d}} - \alpha_i = -\tau_i \dot{x}_i^{\mathrm{d}}$. In addition, define estimation error as $\widetilde{\theta}_i = \hat{\theta}_i - \theta_i$, $\widetilde{\beta} = \hat{\beta} - \beta, \widetilde{f}_{\mathrm{w}} = \hat{f}_{\mathrm{w}} - f_{\mathrm{w}}$.

The derivation of dynamic surface S_1, S_2 can be obtained as follows:

$$\begin{aligned} \dot{S}_1 &= S_2 + z_2 - k_1 S_1 \\ \dot{S}_2 &= S_3 + z_3 - k_2 S_2 \end{aligned} \tag{40}$$

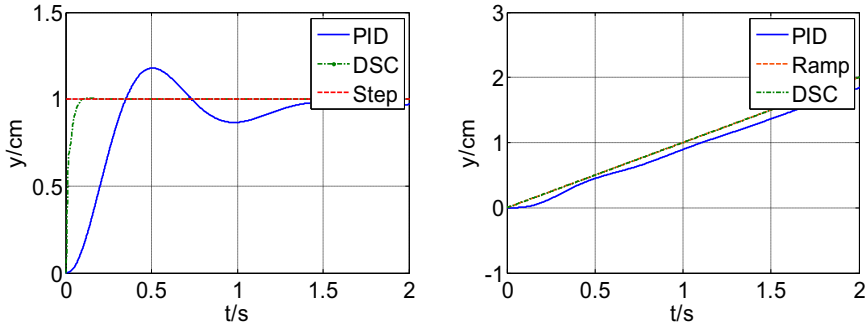

Figure 4. Simulation results of sine signal and ramp signal.

According to the control law and the definition of estimation error,

$$\lambda u = \bar{u} + \lambda\tilde{\beta}\bar{u} \tag{41}$$

Then, simplify $\dot{z}_i$. According to Equations (31), (32) and (33), the following equation can be attained:

$$\dot{z}_{i+1} = -\frac{z_{i+1}}{\tau_{i+1}} + \phi_{i+1}(S_i, x_i) \tag{42}$$

where $\phi_{i+1}(S_i, x_i) = k_i\dot{S}_i + \Sigma((\partial f_i)/(\partial x_k))\dot{x}_k - \ddot{x}_i^{\mathrm{d}}$ and a upper bound of ϕ_i is M_i.

Establish the Lyapunov function of the MDSC controller,

$$V = \frac{1}{2}\left(S_1^2 + S_2^2 + S_3^2 + z_2^2 + z_3^2 + \frac{\tilde{\theta}_1^2}{\xi_1} + \frac{\tilde{\theta}_2^2}{\xi_2} + \frac{\tilde{\theta}_3^2}{\xi_3} + \frac{\lambda}{\gamma_\beta}\tilde{\beta}^2 + \frac{\tilde{f}_{\mathrm{w}}^2}{\gamma_{f_{\mathrm{w}}}}\right) \tag{43}$$

To simplify the derivation of Equation (43), first it is necessary to simplify $S_i\dot{S}_i$.

$$\begin{aligned} S_1\dot{S}_1 &\le S_1^2 + \frac{1}{4}S_2^2 + \frac{1}{4}z_2^2 - k_1S_1^2 \\ S_2\dot{S}_2 &\le S_2^2 + \frac{1}{4}S_3^2 + S_2^2 + \frac{1}{4}z_3^2 - k_2S_2^2 \\ S_3\dot{S}_3 &= -k_3S_3^2 - \tilde{\theta}_1x_1S_3 - \tilde{\theta}_2x_2S_3 - \tilde{\theta}_3x_3S_3 \\ &\quad + f_{\mathrm{w}}S_3 - |S_3|\hat{f}_{\mathrm{w}} + \lambda\tilde{\beta}\bar{u}S_3 \end{aligned} \tag{44}$$

then, transform $z_i\dot{z}_i$,

$$\begin{aligned} z_2\dot{z}_2 &\le -\frac{z_2^2}{\tau_2} + \frac{z_2^2M_2^2}{2\mu} + \frac{\mu}{2} \\ z_3\dot{z}_3 &\le -\frac{z_3^2}{\tau_3} + \frac{z_3^2M_3^2}{2\mu} + \frac{\mu}{2} \end{aligned} \tag{45}$$

where μ is a positive constant. Next, transform $\tilde{\theta}_i\dot{\tilde{\theta}}_i$, $\tilde{\beta}\dot{\tilde{\beta}}$ and $\tilde{f}_{\mathrm{w}}\dot{\tilde{f}}_{\mathrm{w}}$,

$$\begin{aligned} \tilde{\theta}_i\dot{\tilde{\theta}}_i &\le \xi_iS_3x_i\tilde{\theta}_i - \frac{\xi_i\zeta_i}{2}(\tilde{\theta}_i^2 - \theta_i^2) \\ \tilde{\beta}\dot{\tilde{\beta}} &\le -\tilde{\beta}\gamma_\beta\bar{u}S_3 - \frac{\eta_\beta\gamma_\beta}{2}(\tilde{\beta}^2 - \beta^2) \\ \tilde{f}_{\mathrm{w}}\dot{\tilde{f}}_{\mathrm{w}} &\le \tilde{f}_{\mathrm{w}}\gamma_{f_{\mathrm{w}}}|S_3| - \frac{\gamma_{f_{\mathrm{w}}}\eta_{f_{\mathrm{w}}}}{2}(\tilde{f}_{\mathrm{w}}^2 - f_{\mathrm{w}}^2) \end{aligned} \tag{46}$$

Thus, the derivation of the Lyapunov function is

$$\begin{aligned} \dot{V} &\le (2-k_1)S_1^2 + \left(\frac{9}{4} - k_2\right)S_2^2 + \left(\frac{1}{4} - k_3\right)S_3^2 + \mu \\ &\quad + \left(\frac{1}{4} - \frac{1}{\tau_2} + \frac{M_2^2}{2\mu}\right)z_2^2 + \left(\frac{1}{4} - \frac{1}{\tau_3} + \frac{M_3^2}{2\mu}\right)z_3^2 \\ &\quad - \frac{\xi_1}{2}(\tilde{\theta}_1^2 - \theta_1^2) - \frac{\xi_2}{2}(\tilde{\theta}_2^2 - \theta_2^2) - \frac{\xi_3}{2}(\tilde{\theta}_3^2 - \theta_3^2) \\ &\quad - \frac{\lambda\eta_\beta}{2}(\tilde{\beta}^2 - \beta^2) - \frac{\eta_{f_{\mathrm{w}}}}{2}(\tilde{f}_{\mathrm{w}}^2 - f_{\mathrm{w}}{}^2) \end{aligned} \tag{47}$$

choose $c > 0, k_1 \ge 2 + c, k_2 \ge \frac{9}{4} + c, k_3 \ge \frac{1}{4} + c, (1/\tau_i) \ge (M_i^2/2) + \frac{1}{4} + c$, $\zeta_i = (2c/\xi_i)$, $\eta_\beta = (2c/\gamma_\beta)$ and $\eta_{f_{\mathrm{w}}} = (2c/\gamma_{f_{\mathrm{w}}})$. Thus,

$$\dot{V} \le -2cV + \frac{1}{2}(\zeta_1\theta_1^2 + \zeta_2\theta_2^2 + \zeta_3\theta_3^2 + \lambda\eta_\beta\beta^2) + \mu \tag{48}$$

suppose $d = \frac{1}{2}(\zeta_1\theta_1^2 + \zeta_2\theta_2^2 + \zeta_3\theta_3^2 + \lambda\eta_\beta\beta^2) + \mu$, Equation (48) can be written as

$$\dot{V} \le -2cV + d \tag{49}$$

the solution of Equation (49) is as follows:

$$V \le \frac{d}{2c} + \left(V(0) - \frac{d}{2c}\right)\mathrm{e}^{-2ct} \tag{50}$$

suppose p is an upper bound of $V(0)$, the value of V will decay or remain stable all the time if $c \ge (d/2p)$. That means the derivation of V is negative semidefinite and the system can be stable.

3.5. Simulation research of modified dynamic surface control

Several simulation experiments are designed to compare the performance between the DSC controller and the MDSC controller as shown in Figures 5 and 6. First, input force disturbance $F_{\mathrm{w}} = 5 + 5\sin(5\pi t)(N)$ to these two controllers and then observe the position response under step tracking signal and 5 Hz sine tracking signal. Then, add some noise to the feedback channel and view the tracking effects of two controllers. The results of simulation are as follows:

Figures 5 and 6 show that the MDSC controller has a better performance. The DSC controller cannot track the 5 Hz sine signal and step signal when the disturbance force is input. There are overshoot and phase advance in sine signal tracking while large steady-state error in step tracking. When it comes to noise interference, the output of the DSC controller is a little disordered, but the MDSC controller can still track the input signal. Therefore, we can come to the conclusion that MDSC controller has better abilities to resist disturbance and uncertainties.

For further comparison, a simulation experiment is designed to compare our MDSC controller with the controller designed by other scholars. Al-Dhaifallah et al. have proposed a fuzzy fractional-order PID controller for pneumatic pressure regulating system (Al-Dhaifallah, Kanagaraj, & Nisar, 2018). We apply the controller designed by them into our pneumatic position control system and make a comparison between their controller and ours. Input the ramp signal and 2Hz sine signal into these two systems with different controllers, respectively, and the results are shown in Figure 7.

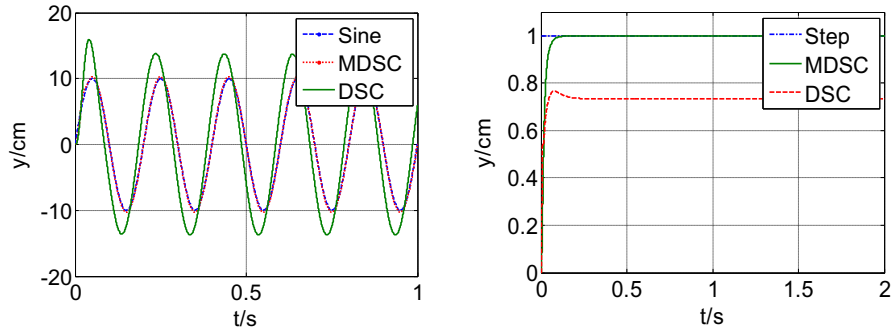

Figure 5. Position response under force disturbance.

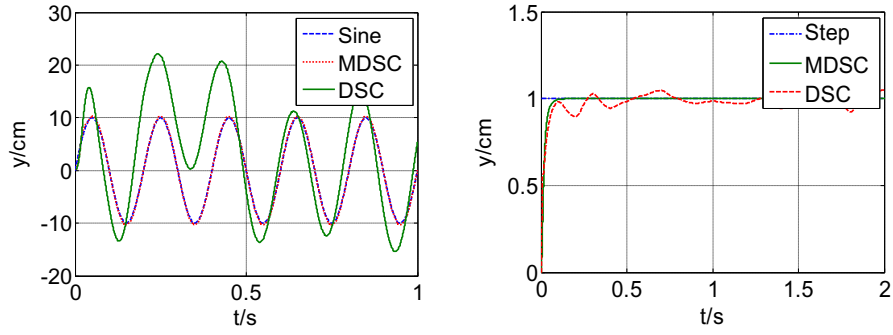

Figure 6. Position response under noise interference.

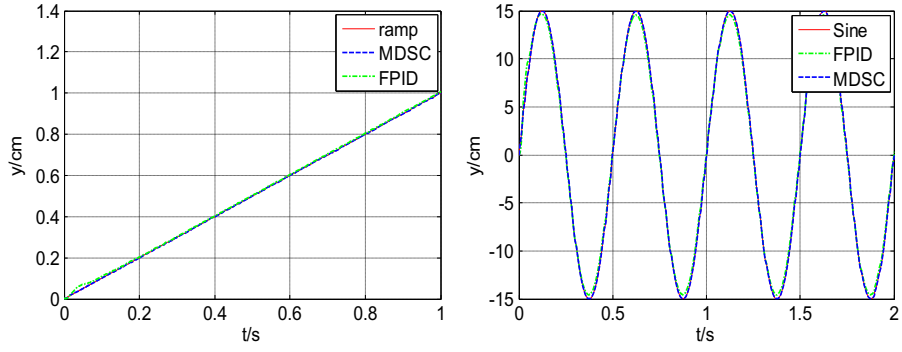

Figure 7. Position response under force disturbance.

From Figure 7, it can be deduced that both two controllers can make the pneumatic system track input signals and have not bad control performance. Besides, the MDSC controller designed by us can accomplish the control tasks of pneumatic systems like other published ones.

4. Experiment on pneumatic compliant system

In this section, two pneumatic experiments are designed to verify the accuracy of previous theories. One is the position step response experiment for comparing the control performance among the traditional PID controller, normal DSC controller and the MDSC controller. The other is the force impulse experiment to test whether MDSC controller has stronger robustness than normal DSC controller as simulation results show.

4.1. Brief introduction about the experimental platform

The whole pneumatic system is controlled by DSP and driven by cylinders. The pressure of intake chamber in the cylinder determines the output position of the system. By controlling the voltage of proportional pressure regulator, the intake chamber pressure can be adjusted to regulate the system output. In addition, the pressure of two chambers in the cylinder can be collected by the proportional pressure regulator. In order to obtain positional information, a position sensor is used. What is more, a two-position and five-port electronic valve is applied to ensure that the cylinder piston can reciprocate. The experimental platform is shown in Figure 8 and the structure of experimental platform is shown in Figure 9.

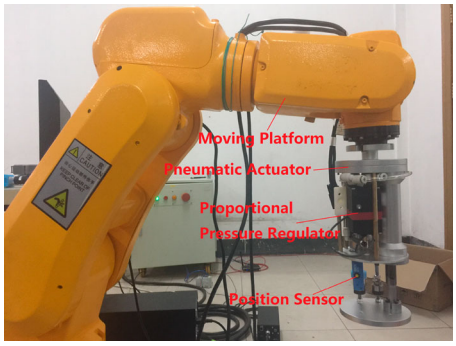

Figure 8. Experimental platform with industrial robot.

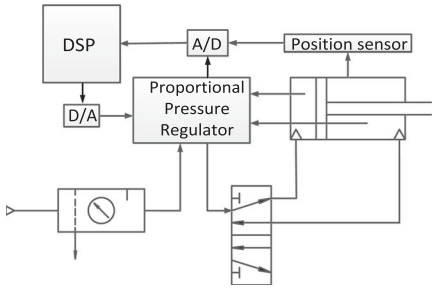

Figure 9. System Structure of experimental platform.

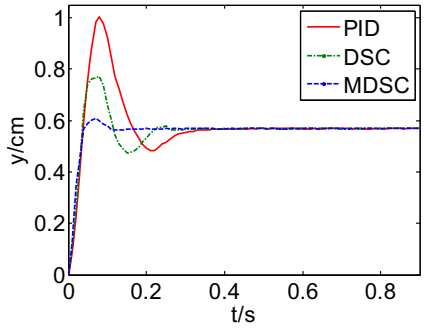

Figure 10. Result of position step response experiment.

4.2. Position step response experiment

A step position signal is input to the system under three different control methods. Fromthe results shown in Figure 10, it is apparent that DSC controller and MDSC controller have less overshoot and shorter adjusting time, which means that these two DSC controllers have better control performance than the PID controller. The step response of the normal DSC controller is worse than that of the MDSC controller. The reason is that the normal DSC controller depends on the mathematic model which cannot be absolutely precise.

4.3. Force impulse experiment

Evert the same force disturbance to the pneumatic system with normal DSC controller and the system with

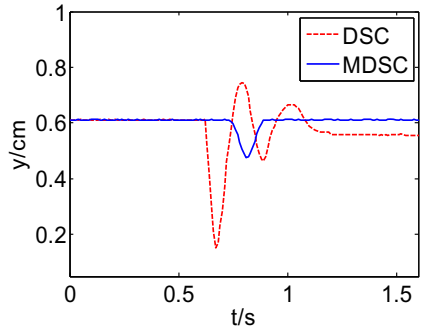

Figure 11. Result of the force impulse experiment.

MDSC controller in the same steady state. Then, observe position response of these two controllers. From the result in Figure 11, the MDSC controller has smaller overshoot, less oscillation times and lower steady-state error. The experiment indicates that the MDSC controller has stronger robustness against external disturbance, which verifies the correctness of simulation results and theoretical analysis.

5. Conclusion

In this paper, an MDSC based on position feedback is developed to try to accomplish pneumatic position servo control. It can effectively resist the adverse effects caused by mathematic model uncertainties, external force disturbance and noise interference on feedback channel in the pneumatic positioning system. The MDSC controller also has better control accuracy, response speed, smoothness and robustness than the normal DSC controller and PID controller, which is verified by the results of simulation and actual pneumatic experiments. Moreover, some other scholars have already put DSC theories into marine vehicles, spacecraft, motor position control and so on recently and get satisfactory control results (Wu, Song, & Sun, 2018; Zhang, 2018). Thus, the MDSC put forward by this paper will be probably applied in these fields and achieve better control performance.

Disclosure statement

No potential conflict of interest was reported by the authors.

Funding

The work is supported by the National Natural Science Foundation of China (61603113, 61703122), the Fundamental Research Funds for the Central University (HIT.NSRIF.201825), the China Postdoctoral Science Foundation (2016M591532), the Heilongjiang Postdoctor Fund (LBH-Z16062), Key Laboratory of Micro-systems and Micro-structures Manufacturing of Ministry of Education, Harbin Institute of Technology (No. 2017 KM008) and the 111 Project (B16014).

References

Al-Dhaifallah, M., Kanagaraj, N., & Nisar, K. S. (2018). Fuzzy fractional-order PID controller for fractional model of pneumatic pressure system. *Mathematical Problems in Engineering*, *2018*, 1–9.

Al-Ibadi, A., Nefti-Meziani, S., & Davis, S. (2017). Novel models for the extension pneumatic muscle actuator performances. *2017 23rd international conference on automation and computing (ICAC)* (pp. 1–6). IEEE .

Chiang, C. J., & Chen, Y. C. (2017). Neural network fuzzy sliding mode control of pneumatic muscle actuators. *Engineering Applications of Artificial Intelligence*, *65*, 68–86.

Dehghan, B., Taghizadeh, S., Surgenor, B., & Abu-Mallouh, M. (2011). A novel adaptive neural network compensator as applied to position control of a pneumatic system. *Intelligent Control and Automation*, *2*(4), 388.

Fathi, M., & Najafi, F. (2017). Improved tracking accuracy of a pneumatic actuator on entire piston stroke by a modified fuzzy-PWM controller. *Journal of the Brazilian Society of Mechanical Sciences and Engineering*, *39*(3), 879–893.

Lin, W., Dong, W., Deng, Y., Qian, C., & Qiu, J. (2016). Contact force modelling and adaptive control of pneumatic system. *Youth academic annual conference of chinese association of automation (YAC)* (pp. 357–362). IEEE.

Raparelli, T., Ivanov, A., & Palladino, F. E. (2017). Textile rotary pneumatic actuator for rehabilitation. *International conference on robotics in Alpe-Adria Danube region* (pp. 727–734). Springer, Cham.

Ren, H. P., Gong, P. F., & Li, J. (2017). Pneumatic position servo control considering the proportional valve zero point. *2017 IEEE international conference on mechatronics (ICM)* (pp. 166–171). IEEE.

Sándor, C., Szabolcs, B., & József, S. (2017). Fuzzy control of antagonistic pneumatic Artificial auscle. *1st agria conference on innovative pneumatic vehicles* (pp. 51–54). At Eger, Hungary.

Schindele, D., & Aschemann, H. (2009). Adaptive friction compensation based on the LuGre model for a pneumatic rodless cylinder. *IECON'09. 35th annual conference of IEEE industrial electronics, 2009* (pp. 1432–1437). IEEE.

Situm, Z., Pavkovic, D., & Novakovic, B. (2004). Servo pneumatic position control using fuzzy PID gain scheduling. *Journal of Dynamic Systems, Measurement, and Control*, *126*(2), 376–387.

Swaroop, D., Hedrick, J. K., Yip, P. P., & Gerdes, J. C. (2000). Dynamic surface control for a class of nonlinear systems. *IEEE Transactions on Automatic Control*, *45*(10), 1893–1899.

Tao, Y. D., & Gu, G. Y. (2017). Design of a soft pneumatic actuator finger with self-strain sensing. *International conference on intelligent robotics and applications* (pp. 140–150). Springer, Cham.

Tong, M., Pan, Y., Li, Z., & Lin, W. (2018). Valid data based normalized cross-correlation (VDNCC) for topography identification. *Neurocomputing*, *308*, 184–193.

Toyama, Y., & Wakimoto, S. (2016). Development of a thin pneumatic rubber actuator generating 3-DOF motion. *2016 IEEE international conference on robotics and biomimetics (ROBIO)* (pp. 1215–1220). IEEE.

Wang, J., Pu, J., & Moore, P. (1999). Accurate position control of servo pneumatic actuator systems: An application to food packaging. *Control Engineering Practice*, *7*(6), 699–706.

Wu, G. Q., Song, S. M., & Sun, J. G. (2018). Adaptive dynamic surface control for spacecraft terminal safe approach with input saturation based on tracking differentiator. *International Journal of Control, Automation and Systems*, *16*(3), 1129–1141.

Zhang, P. (2018). Dynamic surface adaptive robust control of unmanned marine vehicles with disturbance observer. *Journal of Robotics*, *2018*, 1–6.

Zhang, H. X., Wang, W., & Zhang, J. W. (2009). High stiffness pneumatic actuating scheme and improved position control strategy realization of a pneumatic climbing robot. *IEEE international conference on robotics and biomimetics, 2008. ROBIO 2008* (pp. 1806–1811). IEEE.